Transient convective circulation in a sedimented ridge setting: Implications for applying geochemical data to estimate permeability

Peter Alt-Epping[1] and Leslie Smith

Department of Earth and Ocean Sciences, University of British Columbia, Vancouver, B. C., Canada

Received 16 April 2002; revised 24 July 2002; accepted 8 August 2002; published 14 May 2003.

[1] For an open, sedimented ridge setting we investigate by means of transient numerical simulations hydrologic factors that can influence chemical signatures of mineral alteration, and how these features relate to the permeability of the upper oceanic crust. The transient state we consider involves three stages: (1) starting from a static flow field and a conductive thermal regime, flow in basement rocks is initiated as unstable convection; (2) with the inflow of seawater to the basement, the convection pattern evolves into a stable convection cell linking the recharge and discharge sites on the seafloor; and (3) convection weakens through time as the system offsets the initial thermal condition to attain a steady state. The duration of each stage, and the extent of the region in the basement undergoing fluid exchange with seawater varies with permeability. By the end of stage 2, for basement permeabilities between 1×10^{-14} and 1×10^{-13} m^2, most of the basement and the deeper sediments surrounding the discharge zone is hydrologically isolated, but with active recirculation inside this zone. Through-flow of seawater is restricted to a relatively narrow boundary layer. The unstable flow geometry during stages one and two is reflected in fluctuations of recharge and discharge rates into and out of the basement, and periodic variations in temperature of the discharging fluids. Fluid discharge at steady state is approximately one-half of the average occurring during stage one. Changing flow patterns through time lead to a strongly heterogeneous evolution of water/rock ratios in the basement. Average water/rock ratios for the basement approach a log-log linear correlation with basement permeability as steady state is reached. *INDEX TERMS:* 3035 Marine Geology and Geophysics: Midocean ridge processes; 3210 Mathematical Geophysics: Modeling; 5114 Physical Properties of Rocks: Permeability and porosity; 7220 Seismology: Oceanic crust; 8135 Tectonophysics: Hydrothermal systems (8424); *KEYWORDS:* hydrothermal circulation, sedimented ridges, permeability, water-rock ratios

Citation: Alt-Epping, P., and L. Smith, Transient convective circulation in a sedimented ridge setting: Implications for applying geochemical data to estimate permeability, *J. Geophys. Res.*, *108*(B5), 2246, doi:10.1029/2002JB001930, 2003.

1. Introduction

[2] Ocean Drilling Program (ODP) Legs 139 and 169 to Middle Valley, at the northern end of the Juan de Fuca Ridge, provided important insights to the flow conditions in the oceanic basement at a sedimented ridge crest [*Davis et al.*, 1994; *Fouquet et al.*, 1998]. At Middle Valley, the upper oceanic crust is composed of a permeable basement, consisting of sills and lithified sediments, overlain by a thick sequence of low-permeability turbidite sediments. The sediment cover acts as a hydrological seal and a thermal insulator to the underlying crust, leading to temperatures that are on average much higher than in a nonsedimented ridge setting. Fluid exchange between the basement and the ocean is predominantly restricted to sites where higher-permeability pathways breach the sediment cover, such as at fault zones, or where basement is exposed at the seafloor.

[3] A number of studies have addressed the magnitude and distribution of permeability in the upper igneous oceanic crust. A summary can be found in the work by *Fisher* [1998]. Permeability values measured on basalt samples in the laboratory range from 1×10^{-20} to 1×10^{-16} m^2 [e.g., *Christensen and Ramananantoandro*, 1988; *Hamano*, 1980; *Karato*, 1983]. Results from packer tests yield a range of permeabilities from less than 1×10^{-17} [e.g., *Becker et al.*, 1989, Costa Rica Rift] to about 1×10^{-13} m^2 [*Larson et al.*, 1993, Pigafetta Basin]. Relatively high permeabilities (greater than 1×10^{-14} m^2) occur in the uppermost extrusive part of the young basaltic crust [*Fisher*, 1998]. A thin interval in the sediment/sill sequence at Middle Valley was estimated to have a permeability as high as 1×10^{-10} m^2 [*Becker et al.*, 1994].

[4] Numerical models have also been used to estimate the magnitude of permeability in the upper oceanic crust. Calibration constraints include fluid temperatures and flow rates required to form massive sulfide deposits [e.g., *Lowell*

[1]Now at CSIRO—Exploration and Mining, Bentley, Western Australia, Australia.

0148-0227/03/2002JB001930$09.00

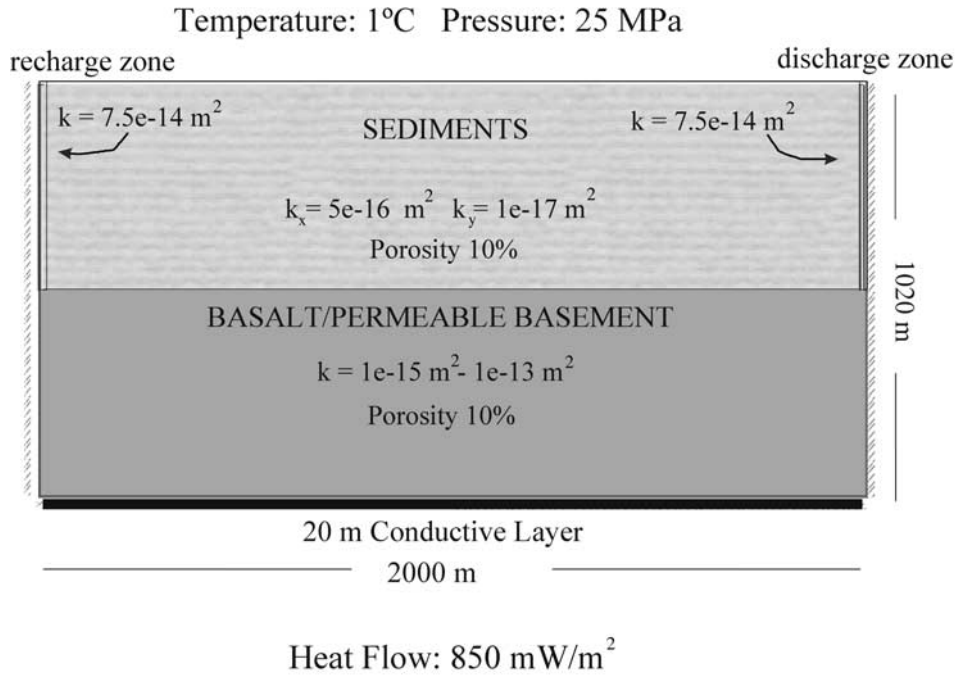

Figure 1. Model flow domain, including initial and boundary conditions and solid medium properties.

and Rona, 1985], seafloor heat flow patterns [e.g., *Rabinowicz et al.*, 1998; *Ribando et al.*, 1976], or the thermal homogenization of a hydrothermal basement in ridge and flank areas [e.g., *Bessler et al.*, 1994; *Davis et al.*, 1996, 1997; *Fisher and Becker*, 1995]. Other model constraints include conditions leading to the formation of megaplumes [*Cann and Strens*, 1989; *Cathles*, 1993; *Lowell and Germanovich*, 1995] or a combination of sealed borehole pressure data, temperature data, and total vent discharge [*Stein and Fisher*, 2001]. These and other means of estimating effective, large-scale permeability [e.g., *Davis et al.*, 1999] yield permeability estimates that are systematically higher than those derived from borehole data.

[5] Despite the expanding database and sophistication of computer models, the magnitude and distribution of permeability in the upper oceanic crust remains poorly known. It appears that an approximately isothermal upper basement surface, as suggested by observations from various ridges, can be created by any form of high Nusselt number hydrothermal circulation regardless of the details of the permeability distribution or anisotropy. To characterize the hydrogeologic properties of the upper oceanic crust, geochemical data may provide constraints beyond those that can be derived from hydrologic and thermal measurements [e.g., *Alt-Epping and Smith*, 2001]. The composition of the fluid and the rock represent the integrated effects of the fluid's reactive history along its flowpath and the reactive history at a particular location, respectively. To make effective use of geochemical data, an understanding of the fluid's flowpath and the timescale of responses to system perturbations is necessary.

[6] The objective of this study is to examine how hydrothermal circulation at an open, sedimented ridge crest may affect the degree and pattern of mineral alteration in basement rocks and in the sediments adjacent to the downflow and upflow zones. The vigor of convection and the duration of hydrologic transients are primarily dependent on the magnitude and distribution of permeability. To assess this dependency, we have calculated the transient state of the system as a function of basement permeabilities while holding boundary conditions, sediment permeability, and all other parameters fixed. The focus of this study is on the geometry of flowpaths, recharge into and discharge from the convective layer, and the spatial distribution of water/rock ratios. Geochemical modeling of mineral alteration is reported elsewhere [*Alt-Epping*, 2000]. While we base a number of the parameter values on data obtained at Middle Valley, the simulations should not be interpreted as representing conditions specific to Middle Valley.

2. Model Design

[7] A two-dimensional numerical analysis of hydrothermal circulation forms the basis of our study. The domain is 2000 m wide and 1020 m deep (Figure 1). It includes 500 m of low-permeability sediments overlying 500 m of a higher-permeability basement unit. A thin layer with very low permeability is located at the base of the domain, where heat transfer is conductive. This layer was initially adopted to improve numerical stability, but it ultimately proved not to be a significant feature of the model structure. On both sides of the domain and penetrating through the sediments are 5-m-wide fracture zones of higher permeability that act as a recharge site for seawater entering the basement or a discharge site for hydrothermal fluids exiting to the ocean. Because of the symmetry of the model domain and boundary conditions, it is not possible to specify a priori which of the two fracture zones will serve as a focused discharge site. To facilitate visual comparison of systems with different permeability, results are always plotted with the recharge zone to the left, and the discharge zone on the right side of the model domain.

[8] A constant fluid pressure of 25 MPa is assigned to the upper boundary, representing the seafloor hydrostat. The isobaric seafloor permits fluid discharge and recharge through the sediment cover. The temperature at the seafloor is 1°C, corresponding to ocean bottom temperature. We assume a constant heat flux of 850 mW/m^2 along the base of the domain, which is within the range of measured heat fluxes at Middle Valley in the vicinity of Leg 139 [*Davis and Villinger*, 1992]. Both sides of the domain are impermeable and adiabatic.

[9] Packer and flowmeter experiments in the basement at Middle Valley indicate that the lowermost 180 m of the sediment/sill sequence in Hole 857D and the upper igneous basement in Hole 858G have an average permeability on the order of 1×10^{-14} m^2 [*Becker et al.*, 1994]. We choose this basement permeability as a base case. These results are then compared to those obtained using higher and lower permeability values. The range of permeabilities considered in this study spans two orders of magnitude, from 1×10^{-15} to 1×10^{-13} m^2. For the domain shown in Figure 1, the lower permeability value is close to the threshold that marks the onset of convective circulation. The higher-permeability value is within the range for which a steady-state convective pattern can develop. Constraints on simulation times due to the small time steps needed to maintain convergence at high permeability did not permit us to consider cases where the basement permeability was higher than 1×10^{-13} m^2.

[10] Bulk permeability measurements on sediment samples from Middle Valley yielded values between $9.9 \times 10^{-17}$and 1.8×10^{-15} m^2 [*Fisher et al.*, 1994]. In-situ estimates of permeability range from about 5×10^{-15} m^2 near the seafloor to about 1×10^{-17} m^2 at 100 m depth. According to *Davis et al.* [1992] and *Rigsby et al.* [1994], the sand/mud ratio in the upper part of Hole 858A is about 1:10. In our model, permeability values in the horizontal and vertical direction are calculated using a permeability value of 5×10^{-15} m^2 for sand and a value of 1×10^{-17} m^2 for the mud fraction. The arithmetic and harmonic mean yield a horizontal and vertical permeability of 5×10^{-16} and 1×10^{-17} m^2, respectively.

[11] The permeability assigned to the recharge and discharge zones is 7.5×10^{-14} m^2. There is no observational constraint for this value. This permeability value was selected so that temperatures of basement fluids in our simulations would be similar to those recorded at Middle Valley. Geologic structures that may control local-scale features around the discharge zone, such as the secondary circulation system proposed for the Dead Dog vent field at Middle Valley [*Stein and Fisher*, 2001], are not included within the model.

[12] For all material properties other than permeability, a simplified representation has been adopted with uniform values assigned to all units. Porosity and rock density are fixed at 10% and 2000 kg/m^3, respectively. In reality, porosity decreases with depth, especially in the upper part of the sediment section, and the density of the basement rock is greater than that of the sediments. The dispersivities are 10 m in the direction of fluid flow, and 1 m in the direction transverse to the velocity vector. The thermal conductivity of the solid phase and the heat capacity are fixed at 1.8 W/m°C and 1000 J/kg°C, respectively. To help stabilize the numerical solution at higher permeability and for high temperature conditions, the rock mass is assumed to be incompressible. The general outcome of the simulations is not influenced by these simplifications, but they must be borne in mind when considering the absolute timescales of the hydrologic and thermal transients presented in the results section. Fluid properties (density, viscosity, thermal conductivity) are calculated using the equations from the ASME Steam Tables [*Meyer et al.*, 1983]. The effect of salinity on the fluid properties is not considered. The governing equations that describe the representation of the hydrothermal flow system and a summary of the finite volume technique used to solve these equations are given in Appendix A.

[13] Choice of the initial condition for the hydrologic and thermal regime is problematic because of the complex and dynamic nature of geologic processes at a ridge crest. The simulations are interpreted in the framework of a transient response to a system perturbation, rather than the evolution of a hydrothermal convection system at a ridge crest. The initial condition is based on a conductive temperature field and a static fluid. This condition leads to an initial excess heat in the system which is then "mined" by fluid convection. *Rosenberg et al.* [1993] showed that the time to establish a steady convection pattern varies with the assumed form of the initial temperature profile, thus, the timescale associated with the early time convection pattern is subject to our choice of the initial condition.

[14] The main simplifications made in developing the simulations are as follows:(1) The basement is represented as a homogeneous porous medium, rather than a unit where flow is focused within a subset of higher-permeability faults or layers; (2) There is no feedback on permeability from chemical reactions, tectonic processes, sediment deposition or compaction. In reality, each of these may modify the flow system.; (3) The model is two-dimensional. In reality, the flow geometry is three dimensional with asymmetrical cells of plume-like ascending flow and sheet-like descending flow [e.g. *Lister*, 1990; *Rabinowicz et al.*, 1998]. Discharge is localized to discrete areas, rather than forming linear features, as is implicit in a two-dimensional model; (4) A fixed temperature along the seafloor results in an overestimate of temperature gradients in the upper part of the discharge zone; (5) The assumption of a constant heat flux over thousands of years implies that the heat source at depth is replenished.

3. Hydrothermal Circulation in an Open Sedimented Ridge Setting

[15] Figures 2, 3and 4 illustrate the fluid flow and temperature fields for a basement permeability of 1×10^{-15}, 1×10^{-14}, and 1×10^{-13} m^2, respectively. The behavior of the convective system shows similar characteristics at each permeability; the main differences are in the timescale of effects and the magnitude of and variation in temperature and fluid velocity. The response of the system can be divided into three stages. For each permeability, we have selected snapshots in time that best illustrate the character of flow during each stage. In stage 1, flow is initiated and unstable convection cells with a low aspect

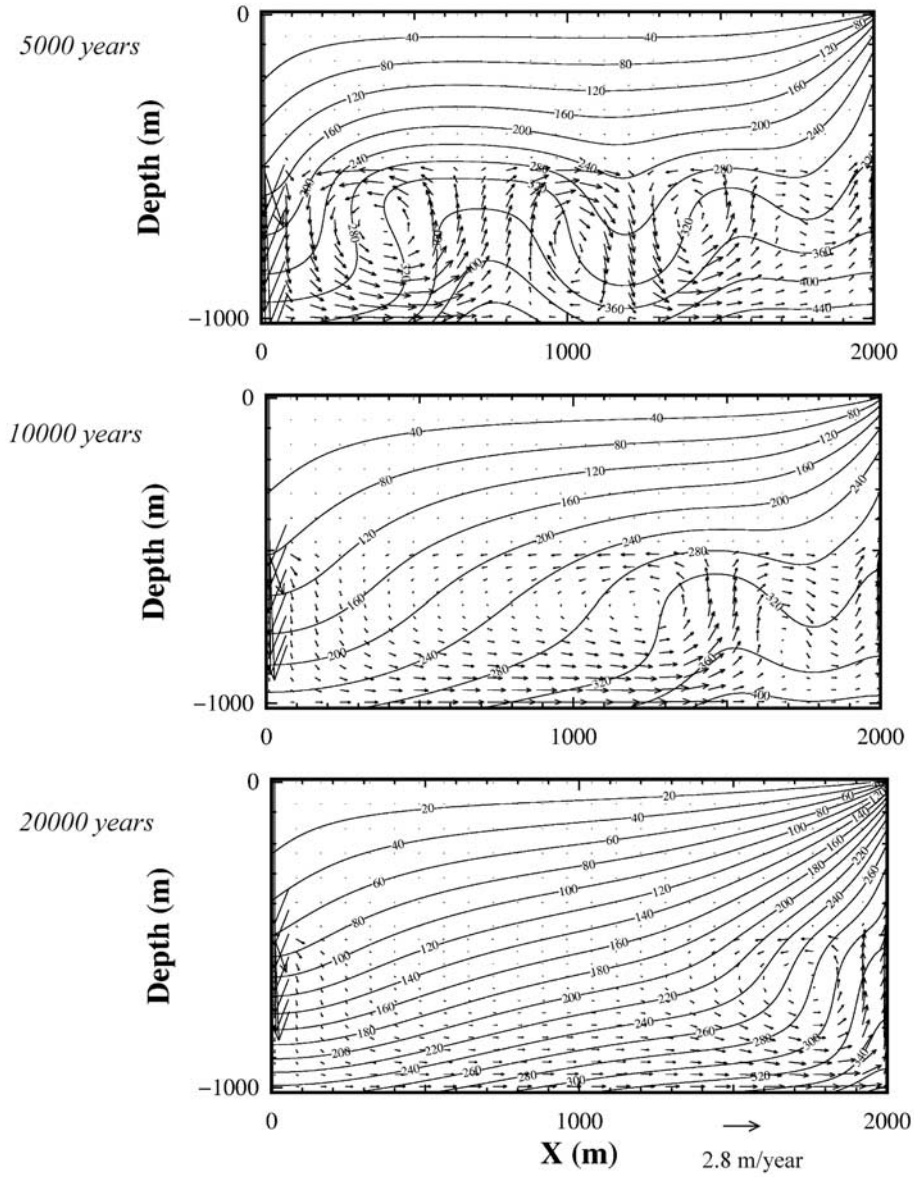

Figure 2. Evolution of temperature and velocity fields—basement permeability 1×10^{-15} m^2.

ratio (width:height) develop (upper panels, Figures 2, 3 and 4). For a permeability of 1×10^{-13} m^2, the early flow field is irregular, convection cells are poorly defined, and flow is vigorous enough to thermally homogenize the basement. Temperatures between the bottom boundary and the sediment/basement interface do not vary by more than 20°C. The thermal structure in the basement reflects the fluid flow patterns. For a permeability of 1×10^{-15} m^2, and to some degree 1×10^{-14} m^2, a wave-like variation in the isotherms extends a considerable distance upward into the sediment layer. Stage 1 ends when the continuous inflow of cold seawater creates a thermal plume that enters the basement. The first stage lasts approximately 5000 years for a basement permeability of 1×10^{-15} m^2 and a significant fraction of this time (approximately 3000 years) reflects the sluggish initiation of flow. The duration of stage 1 is reduced by a factor of 10 for a permeability of 1×10^{-14} m^2, and a factor of 50 for a permeability of 1×10^{-13} m^2. By the end of stage 1, the influence on the fluid flow pattern of the assumed static initial condition has largely dissipated.

[16] In stage 2, the convection pattern changes dramatically. The number of convection cells decreases as the cell adjacent to the recharge zone expands (middle panels, Figures 2, 3 and 4). The front of the plume exhibits high temperature gradients and it separates the basement into a region of relatively low fluid temperatures within the plume and a region of higher fluid temperatures outside the plume. The result is a considerable temperature change over a short period of time in regions affected by this thermal plume. The front of the thermal plume moves at a rate that is slower than the ingressing fluid of modified seawater

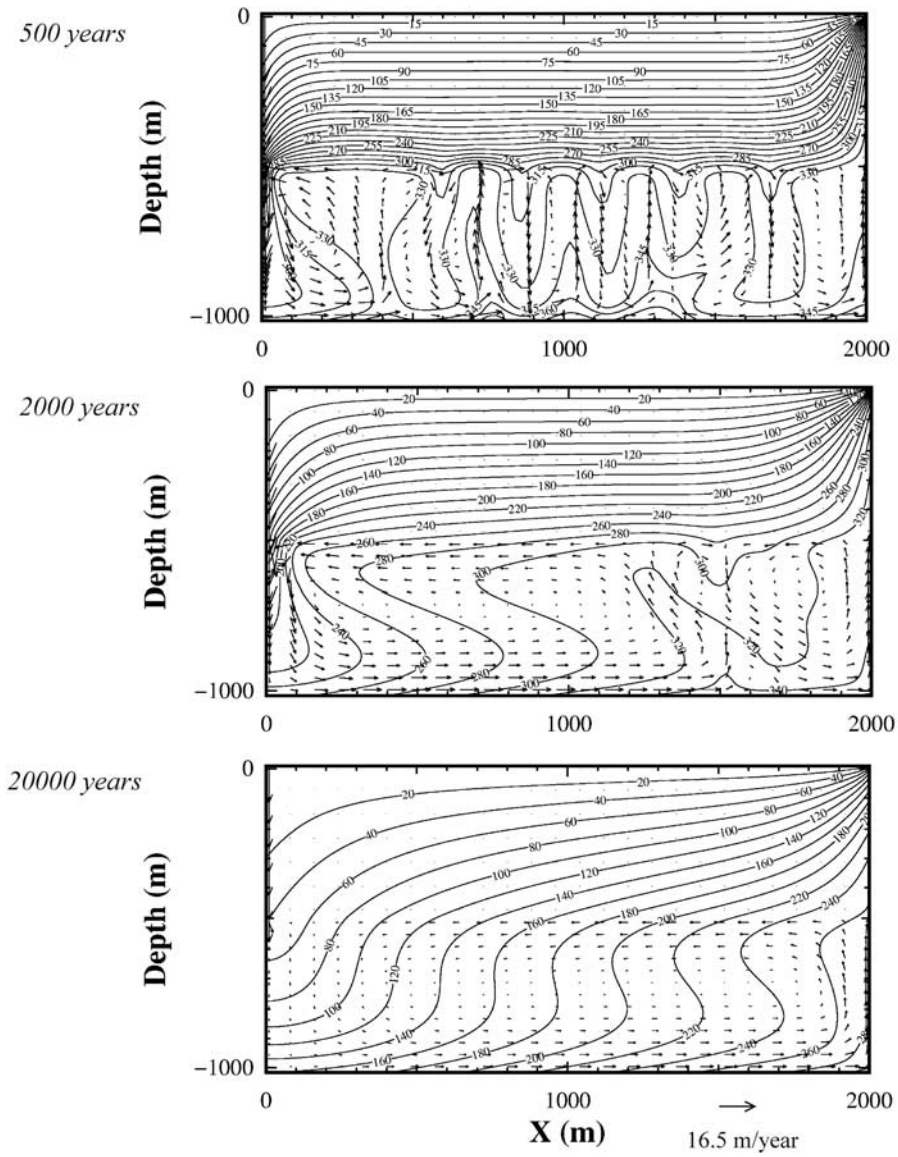

Figure 3. Evolution of temperature and velocity fields—basement permeability 1×10^{-14} m^2.

composition by a factor equivalent to the porosity. Stage 2 ends once a single, stable convective cell forms that links the recharge and discharge sites on the seafloor. Relative to the case with a permeability of 1×10^{-15} m^2, the duration of stage 2 is reduced by a factor of 5 for a permeability of 1×10^{-14} m^2, and a factor of 11 for a permeability of 1×10^{-13} m^2.

[17] Despite the stable flow pattern by the end of stage 2, the convective system is not at steady state; during stage 3, the overall vigor of convection continues to decrease as excess heat introduced through the conductive initial condition is removed from the system. The steady-state flow and thermal fields for a permeability of 1×10^{14} and 1×10^{-13} m^2 are shown in the lower panels of Figures 3 and 4, respectively. As will be evident in a later figure, for a permeability of 1×10^{-15} m^2 (Figure 2, lower panel), the system has yet to reach its steady state at 20,000 years. Compared to the situation in stages 1 and 2, the single convection cell in the basement leads to a more uniform lateral thermal gradient within the sediment layer that is inversely proportional to the magnitude of the basement permeability.

[18] At a permeability of 1×10^{-14} and 1×10^{-13} m^2, the single convection cell creates a narrow zone for fluids that recharge, pass through, and exit the basement. Near the center of this cell a region of near-stagnant flow is created, where earlier in stages 1 and 2, circulation was vigorous. Hot fluids ascend from the bottom boundary and either exit the system through the discharge zone or become "recycled" in the basement. The highest fluid velocities occur with horizontal flow in this boundary layer and in the region of upward flow. The highest fluid temperatures in the domain occur at the bottom boundary below the discharge zone. The high flow velocities in the regions of upward flow

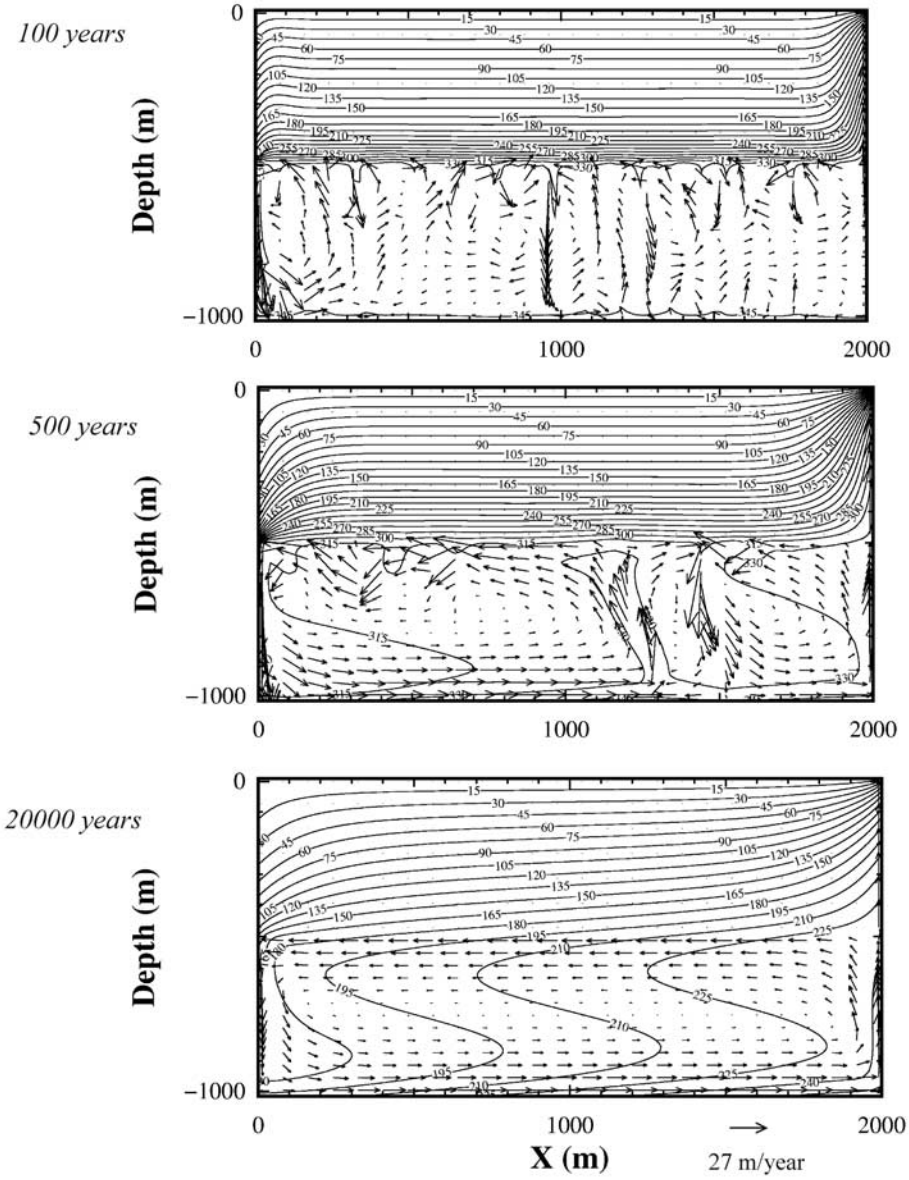

Figure 4. Evolution of temperature and velocity fields—basement permeability 1×10^{-13} m^2.

result in low temperature gradients so that fluids exiting the domain undergo only limited cooling during their ascend toward the seafloor. At a permeability of 1×10^{-15} m^2, the convection cell is confined to the right side of the domain (Figure 2). We return to a discussion of this behavior in a later section of the paper.

[19] The transient flow response seen in Figures 2, 3, and 4 is quite different in the case of a sealed basement without localized sites for fluid exchange at the seafloor [*Ibaraki and Smith*, 1997]. In this setting, for the same permeability range from 10^{-15} to 10^{-13} m^2, the irregular flow pattern in stage 1 evolves into a series of stable, low aspect ratio cells, with a larger number of cells at higher permeability values. A somewhat parallel interpretation of stages 2 and 3 relates to the scenario where normal faulting opens a pathway through the sediment seal and permits cross-flow through the basement, which may then override an existing low aspect ratio convection system.

4. Average Basement Temperature and Temperature Within Recharge and Discharge Zones

[20] The response of the average basement temperature (the average temperature for all nodes in the numerical grid located below 500 m) and the temperature in the recharge and discharge zones 50 m above the sediment-basement interface are illustrated in Figure 5. Calculations for the discharge zone are presented at this location to minimize the influence of the fixed temperature applied along the seafloor. The variation in average basement temperature, and the temperature within the recharge and discharge zones,

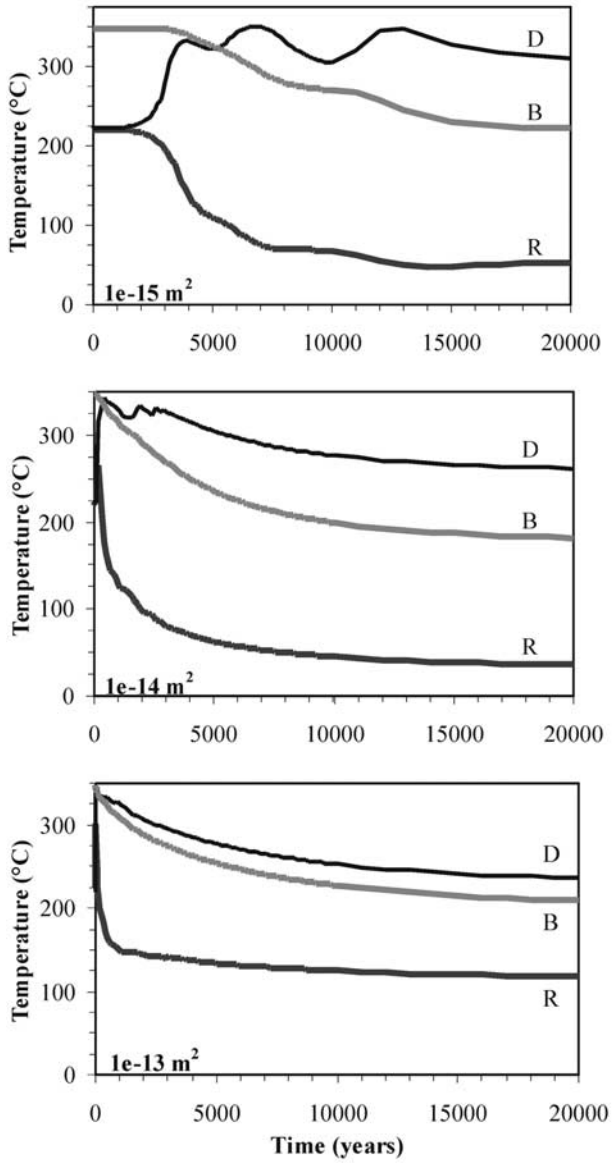

Figure 5. Temperature evolution at the recharge (R) and discharge zones (D) and of average basement temperatures (B).

reflects the three stages of convection identified earlier. The character of temperature variations in each stage is most easily seen for a permeability of 1×10^{-15} m^2. In stage 1, temperatures remain essentially constant until convection is initiated, and then there is a substantial drop in temperature within the recharge zone as seawater approaches the sediment-basement interface, and a substantial rise in temperature within the discharge zone as fluids start to move upward. In the discharge zone, temperature increases from about 220° to 340°C within the first 1000 years after the onset of fluid motion.

[21] Stage 2, which corresponds to the growth of a single convection cell in the basement, is characterized by low-amplitude temperature fluctuations. For a permeability of 1×10^{-15} m^2, these fluctuations in the discharge zone are up to 25°C, with a period on the order of thousands of years. Temperature fluctuations are smaller, with a shorter period, at higher basement permeability; at a permeability of 1×10^{-13} m^2, the fluctuations are barely detectable. The termination of the high temperature state within the discharge zone corresponds to the end of the stage 2 convection pattern.

[22] Stage 3 is marked by a slow decline in temperature as heat continues to be removed from the system and the vigor of convection weakens. At 20,000 years, the average temperature in the basement differs by about 40°C for the permeability range we consider. Where steady state has been reached, the average basement temperature is greater at higher permeability. The temperature at the base of the recharge zone is greater for higher basement permeability; the difference amounts to almost 100°C for a permeability between 1×10^{-15} and 1×10^{-13} m^2. The temperature at the base of the discharge zone tends to be lower at higher basement permeability, but the values fall into a relatively small range. The temperature differences are about 40°C between permeabilities of 5×10^{-15} and 1×10^{-13} m^2. This relatively small range of temperatures for the discharge zone suggests that the temperature of vent fluids, which controls the formation of massive sulfides, does not appear to be primarily dependent on the basement permeability or the vigor of convection. The main factor controlling the discharge temperature in these simulations is the basal heat flux.

[23] Large temperature differences at the recharge zone and relatively similar temperatures at the discharge zone indicate that a substantially larger temperature gradient across the domain exists at lower basement permeabilities. For a permeability of 5×10^{-15} m^2, for instance, this difference amounts to 265°C, whereas for a permeability of 1×10^{-13} m^2 this difference is only 120°C. Thus at lower basement permeabilities, a parcel of fluid undergoes a much greater temperature increase as it travels from the recharge zone to the discharge zone. This large temperature change is likely to lead to chemical alteration patterns that are more heterogeneous at lower basement permeability than at higher permeability.

5. Fluxes Through Recharge and Discharge Zones and Across the Sediment/Basement Interface

[24] Fluctuations of discharge rates and venting temperatures during the early state of an oceanic hydrothermal system have been observed [*Von Damm*, 1995]. To examine the variation of recharge and discharge rates for the hydrothermal basement, the total mass flux is calculated through the recharge zone, entering the discharge zone, and across the sediment/basement interface (Figure 6). Fluxes through the 5-m-wide recharge and discharge zones are determined at a depth of 500 m. Variations in flux rates through time track the three stages of convection described earlier. At the discharge zone, the variations in flux correlate with changes in temperatures; higher fluxes are associated with a higher discharge temperature. For a permeability between 5×10^{-15} and 1×10^{-13} m^2, the fluid discharge at steady state is 45–50% less than that occurring during stage 1.

[25] At steady state, inflow rates through the recharge zone are similar for basement permeability in the range from 5×10^{-15} to 1×10^{-13} m^2. Below this permeability range, near the threshold for the onset of convection, the inflow

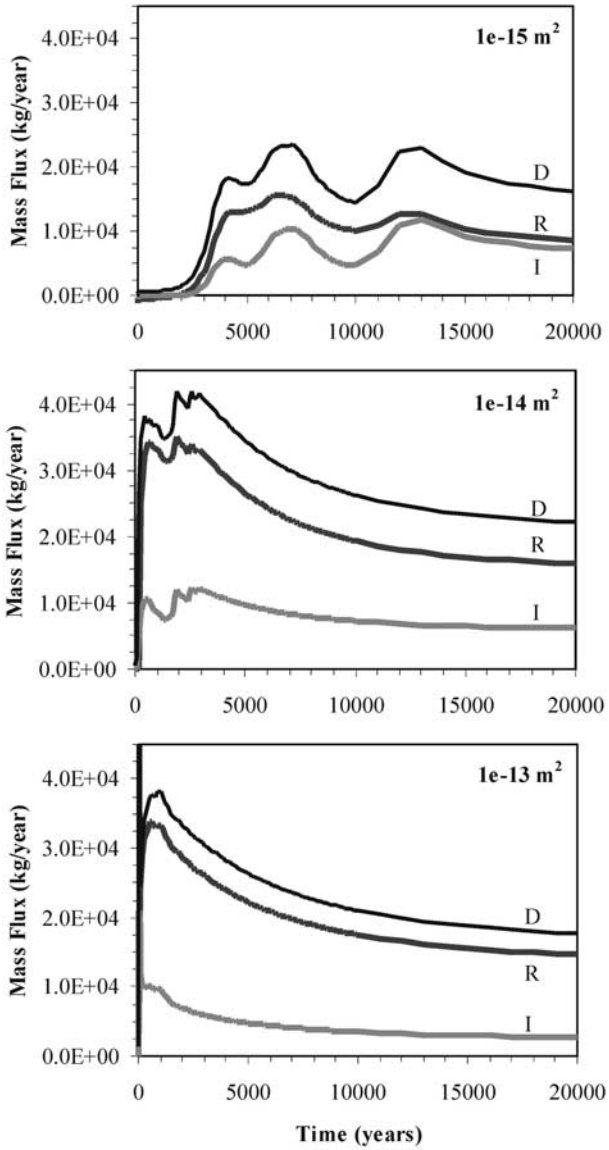

Figure 6. Fluid mass fluxes (kg/yr) through the recharge (R) and discharge zones (D) and across the sediment/basement interface (I).

rate is lower. Net recharge across the sediment-basement interface is higher at lower basement permeability. For a basement permeability of 1×10^{-13} m^2, fluid infiltration from the sediment layer is a small proportion of the total recharge; at 1×10^{-15} m^2, it contributes a nearly equal fraction to the total recharge as does the flow entering through the recharge zone (Figure 6). Leakage is greater through the sediment cover at lower basement permeability because there is greater sub-hydrostatic fluid pressure along the sediment-basement interface. Three implications follow: (1) flow through the discharge conduit relative to that in the recharge zone will be more vigorous, especially at lower values of basement permeability, (2) there is the expectation of a more pronounced geochemical fingerprint of the sediments in the composition of the vent fluids at lower basement permeability, and (3) the interaction between convection in the basement rocks, and the induced leakage across the sediments, leads to a higher fluid discharge from the system at mid-range permeabilities on the order of 1×10^{-14} m^2, with lower fluid discharges at both lower and higher permeabilities.

[26] In stages 1 and 2 of the convective system, temporal variations in flow rates through the sediments are substantive enough to affect the discharge rates of the fluid. The different leakances through the sediment layer also explains why for a higher basement permeability there is a decrease in the total flux entering the discharge zone (by ~15% over the permeability range from 5×10^{-15} to 1×10^{-13} m^2).

6. Flowlines and Travel Times

[27] The flow path of a fluid packet has an important control on the fluid's reactive history [*Norton*, 1978]. As the fluid packet travels through the flow system, it experiences continuous compositional changes as temperature, pressure, and the composition of the rock varies along the flow path. Because fluid pathways and fluid residence times during the transient evolution of system are specific to the assumed initial condition and the lateral distance between the recharge and discharge sites, quantitative inferences on this state are not readily generalized. In broad terms, seawater reaching the basement through the recharge zone during stage 1 or 2 follows a complex path through the basement as it is incorporated within the unstable convection pattern. A pathway of a solute particle released at the seafloor at the recharge zone at the beginning of stage 1 is shown as a dotted line in Figure 7, middle and lower panels. The large amplitude of the "waves" and the crossing of the flowpath (Figure 7, middle panel) suggest that during stages 1 and 2 there will be a greater potential through time for fluids to interact with rocks of different composition, and a rock volume may interact with fluids of different composition (e.g. a fluid of seawater composition or a hydrothermal fluid that is at local equilibrium with the rock). An increase in basement permeability and the vigor of convection leads to smaller and highly unstable convection cells that are more likely to create a thermally and compositionally well-mixed basement, limiting the potential for chemical mass transfer between the solid and aqueous phases (Figure 7, lower panel). This situation leads to a more uniform alteration mineralogy within the basement rocks. The thermal and compositional homogenization at higher basement permeabilities suggests that the overall intensity of alteration may not be correlative with the vigor of convection during stage 1 or 2.

[28] In stage 3, seawater entering the basement through the recharge zone, and the great majority of the water seeping downward from the sediment layer, follows a more regularized flow path. To characterize fluid pathways at the end of stage 3, when the system is at or near steady state, we track fluids by placing particles at the seafloor with equal spacing, and along the length of the recharge and the discharge zones. Particles released along the recharge and the discharge zone indicate the pattern of lateral fluid exchange with the sediments. Figure 7 shows seawater moving through the basement along the outer margin of the convection cell, and exiting the system through the discharge zone after a single pass. Note that this figure has been designed to illustrate path lines between recharge and discharge sites; it is not equiv-

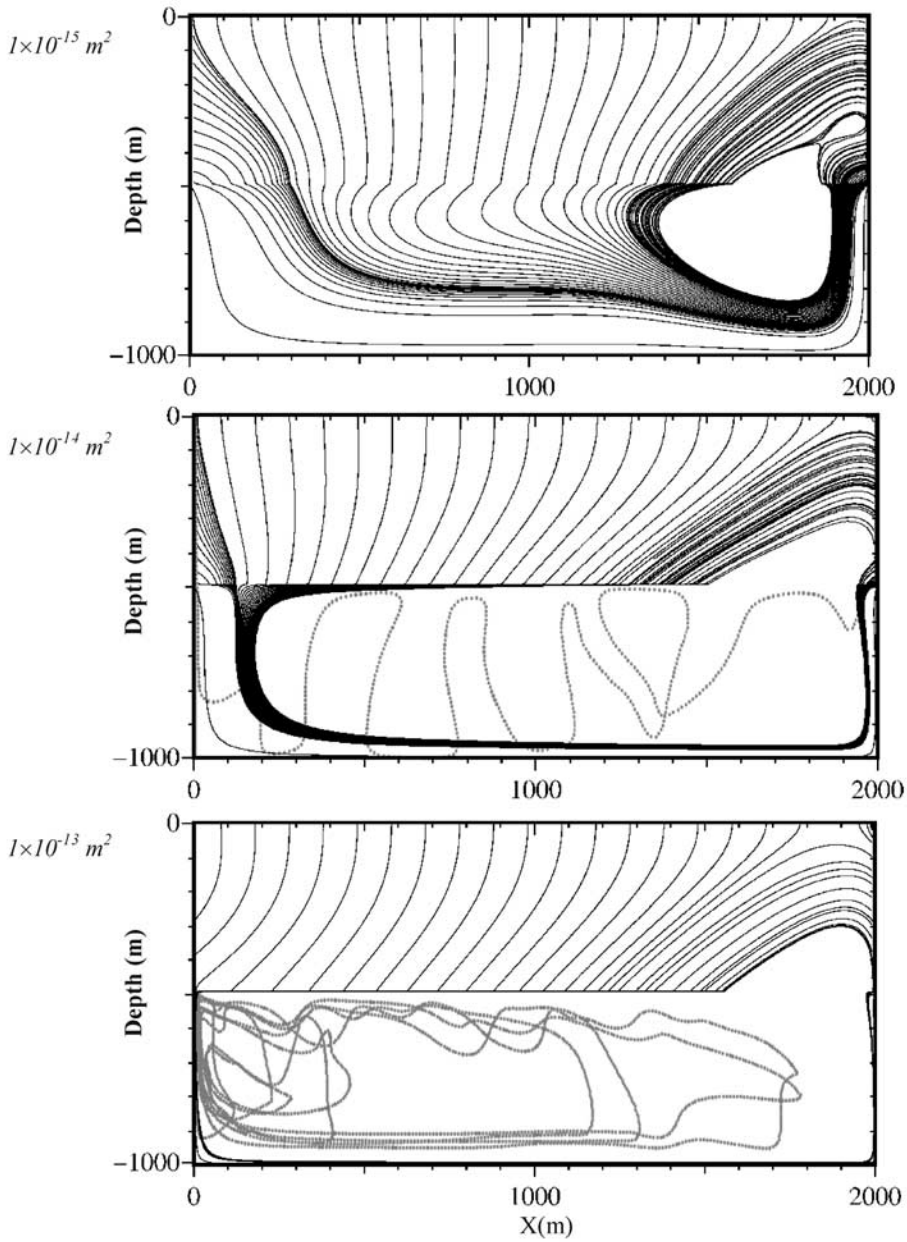

Figure 7. Particle flowpaths for steady-state flow field (solid lines) for basement permeabilities 1×10^{-15} m^2, 1×10^{-14} m^2, and 1×10^{-13} m^2. The dotted flowpaths in the middle and lower panels are calculated starting at the time of perturbation.

alent to a flow net (stream function plot), where the spacing of flowlines is indicative of the local volumetric flux. For a 2000-m separation between the recharge and discharge sites, seawater entering the basement exits the system after 3100, 950 and 210 years for a basement permeability of 1×10^{-15}, 1×10^{-14}, and 1×10^{-13} m^2, respectively. Seawater infiltrating through the sediment layer has a travel time that varies with the path length across the sediment layer. At $x = 1000$ m, the travel time is on the order of 12,500, 14,500, and 30,000 years for the systems with a basement permeability of 1×10^{-15}, 1×10^{-14}, and 1×10^{-13} m^2, respectively. If dispersion were accounted for, these times would correspond to average travel times of solutes. Fluid velocities through the sediments at 20,000 years, calculated at $x = 1000$ and 80 m below the seafloor are 1.7, 3.1, and 3.5 cm/yr for permeabilities of 1×10^{-13}, 1×10^{-14}, and 1×10^{-15} m^2, respectively. There is no advective exchange of through-flowing fluid with the interior of the convection cell, creating a hydrologically isolated zone. The flow geometry is similar to a single pass fracture-loop model [e.g., *Bodvarrson and Lowell*, 1972], in which seawater passes through the system only once.

[29] At a permeability of 1×10^{-15} m^2, the core of the zone that is hydrologically isolated has a width of about

300 m; at a permeability of 1×10^{-13} m^2 it extends across almost the entire width of the domain. As a consequence, the extent of the region in the basement undergoing fluid exchange with seawater varies with permeability. At high permeability only a narrow zone of fluid recharge in the basement exists. At a permeability of 1×10^{-15} m^2 two thirds of the basement undergoes exchange with seawater entering through the recharge zone or the sediments. The reduced flow velocity and higher fluid temperatures toward the discharge zone promotes local chemical equilibrium between the fluid and the rock.

[30] Figure 7 indicates that as fluids ascend through the discharge zone, there is lateral flow into the sediments. After entering the sediments fluid movement is downward toward the basement, resulting in a triangular region affected by lateral flow. The size of this region is similar for all permeabilities, it has a width of 600–800 m at the sediment/basement interface. If all recharging fluids pass through the steady state convective system only once, then the triangular region of lateral flow surrounding the discharge zone is part of the hydrologically isolated convective system. The upper panel shows that at a basement permeability of 1×10^{-15} m^2, a small isolated convection cell forms within this triangle.

[31] The extent and direction of lateral flow at the recharge zone is dependent on basement permeability. At a permeability of 1×10^{-15} m^2, fluid flow from the recharge zone into the sediments affects a triangular region measuring about 400 m in width at the sediment/basement interface. At a permeability of 1×10^{-13} m^2 fluid flow is from the sediments toward the recharge zone. In general, fluids in the sediments tend to move toward the downflow limb of the convection cell in the basement. As the basement region affected by fluid recharge is narrow at higher permeabilities, the downflow limb is located closer to the recharge zone. Thus there is a stronger tendency of lateral fluid motion toward the recharge zone in the sediments at higher basement permeabilities.

[32] Lateral flow of hydrothermal fluids from the discharge zone into the sediments creates a situation where these fluids can be expected to be compositionally distinct from the sediment pore waters and in strong disequilibrium with the mineralogy of the sediments. This flow will create pore water anomalies and distinct mineral alteration patterns. Alteration reactions should be most significant near the seafloor and along the outer margin of this triangular zone due to high temerature gradients and the possible interaction with downflowing seawater/sediment pore water. The triangular shape of the zone affected by lateral flow is consistent with alteration patterns observed at Middle Valley (ODP Site 858 [*Leybourne and Goodfellow*, 1994]).

7. Water/Rock Ratios

[33] Water/rock ratios (w/r) are an expression of time-integrated fluid mass fluxes through a unit mass of rock. Estimates of w/r ratios are typically based on isotope systematics [e.g., *Taylor*, 1977; *Valley*, 1986], a chemical species that is leached from the rock [e.g., *Gillis and Robinson*, 1990], or reaction progress [*Ferry*, 1978]. Water/rock ratios provide a link between hydrological and chemical properties of the system. Our focus is on the pattern and distribution of time-integrated fluid fluxes, expressed as the total fluid mass flux per unit volume of rock. Numeric values of this w/r ratio can be converted to a more conventional form (mass/mass) by dividing by rock density. Water/rock ratios derived from chemical data provide estimates of the physically based w/r ratios, we calculate directly from the simulations [e.g. *Alt-Epping and Smith*, 2001].

[34] Contrary to the instantaneous view of the velocity field, w/r ratios represent the integrated effects of flow conditions. The w/r ratio can be calculated on a cell-by-cell basis in the finite volume mesh, by summing the cumulative inflow to each cell. The variation in the w/r ratio across the basement will map, for a hydrologic perspective, regions where strong chemical alteration may be expected. A comparison of both the velocity and the w/r ratio field demonstrates the degree to which the current flow (and temperature) field is out of equilibrium with the past flow (and temperature) history. If the disequilibrium is significant, we can anticipate that the rock composition, which may preserve the history of physical and chemical conditions, will also be discordant with the current flow and thermal condition.

[35] Figure 8 illustrates the strongly heterogeneous evolution of w/r ratios for a basement permeability of 1×10^{-14} m^2. We do not illustrate w/r ratios for the sediment layer, but simply note that the values are typically several orders of magnitude lower than in the basement layer [*Alt-Epping*, 2000]. During the early, highly irregular state of flow (upper panel), the spatial distribution of w/r ratios reflects the overall flow geometry. The snapshot at 500 years incorporates about 400 years of unstable convection, with the first 100 years required to initiate fluid flow throughout the basement from the static initial condition. The flow pattern leads to vertically oriented, elongated, patch-like zones of higher w/r ratios. The vigorous convection does not, however, lead to substantial spatial gradients in w/r ratios. The situation changes in stage 2, when cooler seawater enters the basement and the single convection cell begins to form (Figure 8, middle panel). This convection cell overprints the initial, patchy distribution of the w/r ratio. This process occurs particularly fast in the outer regions of the convection cell where the highest fluid velocities are present. Because fluid velocities decrease toward the interior of the cell, the initial pattern of w/r ratios tends to be preserved in the central region of this layer. The distribution of w/r ratios is out of equilibrium with the current velocity distribution; fingerprints of the early state, highly vigorous convection are still detectable at much later times.

[36] By 20,000 years the stable convection pattern has overprinted most traces of the initial flow geometry, except for some small patches in the center of the cell (Figure 8, lower panel). The geometry of the w/r ratio contours is now in general accord with the velocity field, with the greatest difference occurring below the recharge zone. The velocity differences between the inner and boundary regions of the convection cell lead to increasingly steeper gradients in the w/r ratio as time progresses. The distinctly higher w/r ratios below the discharge and recharge zones should be detectable in the rock's composition, in particular, below the recharge zone, where cool fluids with a strong chemical seawater component enter the basement in a strong disequi-

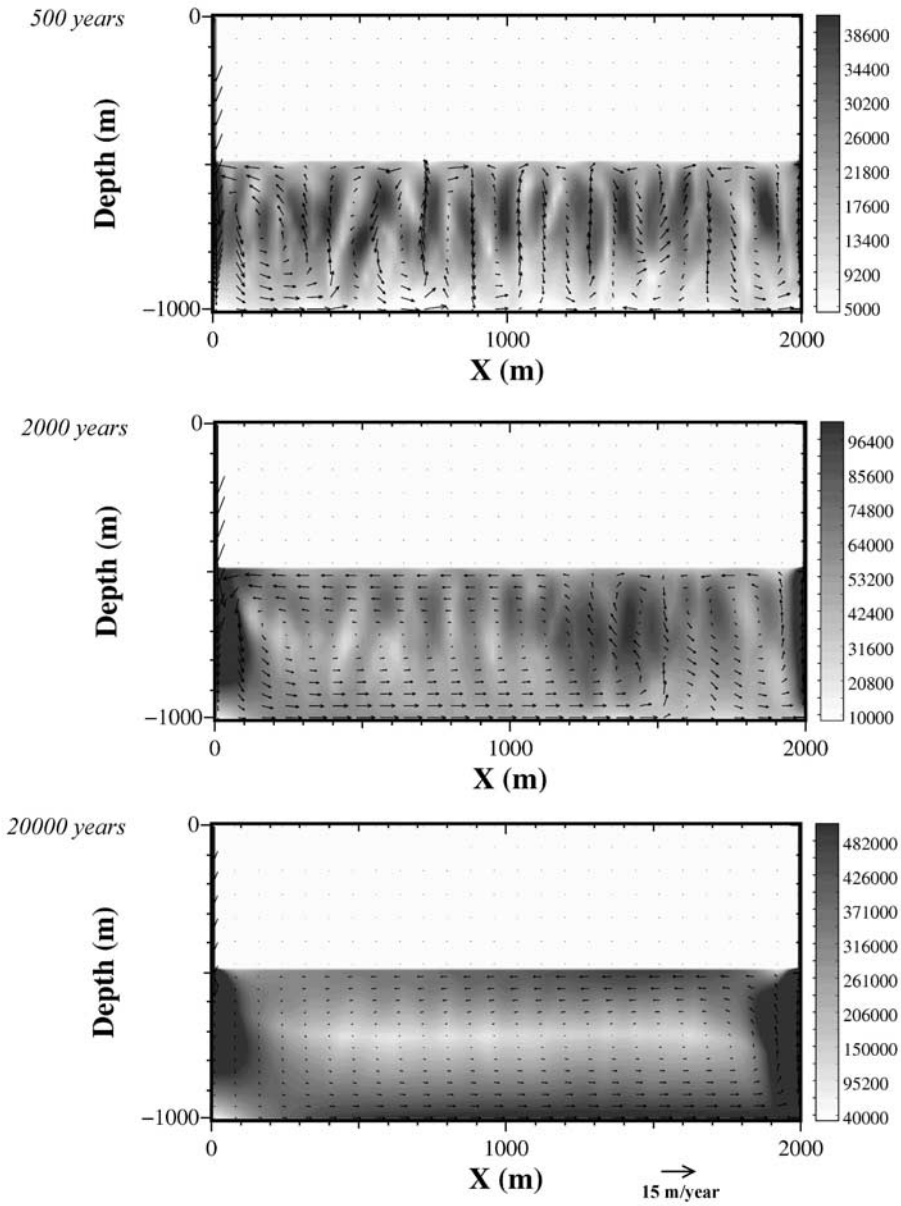

Figure 8. Evolution of water/rock ratios (fluid mass (kg)/volume of rock (m^3))—basement permeability 1×10^{-14} m^2.

librium with the rock. The result of such focused flow will be localized zones of strong chemical alteration.

[37] Similar trends in the w/r ratio are observed at permeability values of 1×10^{-15} and 1×10^{-13} m^2. Figure 9 shows the distribution of the w/r ratio at 20,000 years. Due to the sluggish evolution of the flow field and the extended transient state, at a permeability of 1×10^{-15} m^2, the velocity and the w/r ratio distribution are still in significant disequilibrium (upper panel). The initial sluggish flow and much larger region affected by seawater recharge creates moderate w/r ratio gradients below the recharge and discharge zones. The fluid circulation leads to a zone of near-fluid stagnation at the sediment/basement interface, adjacent to the recharge zone. The main differences between w/r ratios for different permeabilities occur and become more significant toward the outer regions of the convection cell. For instance, the basement with a permeability of 1×10^{-13} m^2 exhibits w/r ratios in the boundary region of the convection cell that are more than twice as high as for a permeability of 1×10^{-14} m^2 (lower panel).

[38] Figures 8 and 9 indicate how the distribution and range of w/r ratios varies with the permeability of the basement. The question arises if there is a single parameter that can express the dependency of w/r ratios on basement permeability. One possibility is to calculate average w/r ratios for the entire basement section. For steady-state conditions, average w/r ratios increase linearly with time for a given basement permeability [*Alt-Epping*, 2000]. Figure 10 shows the average w/r ratios for different permeabilities at a given time. This plot contains curves for a

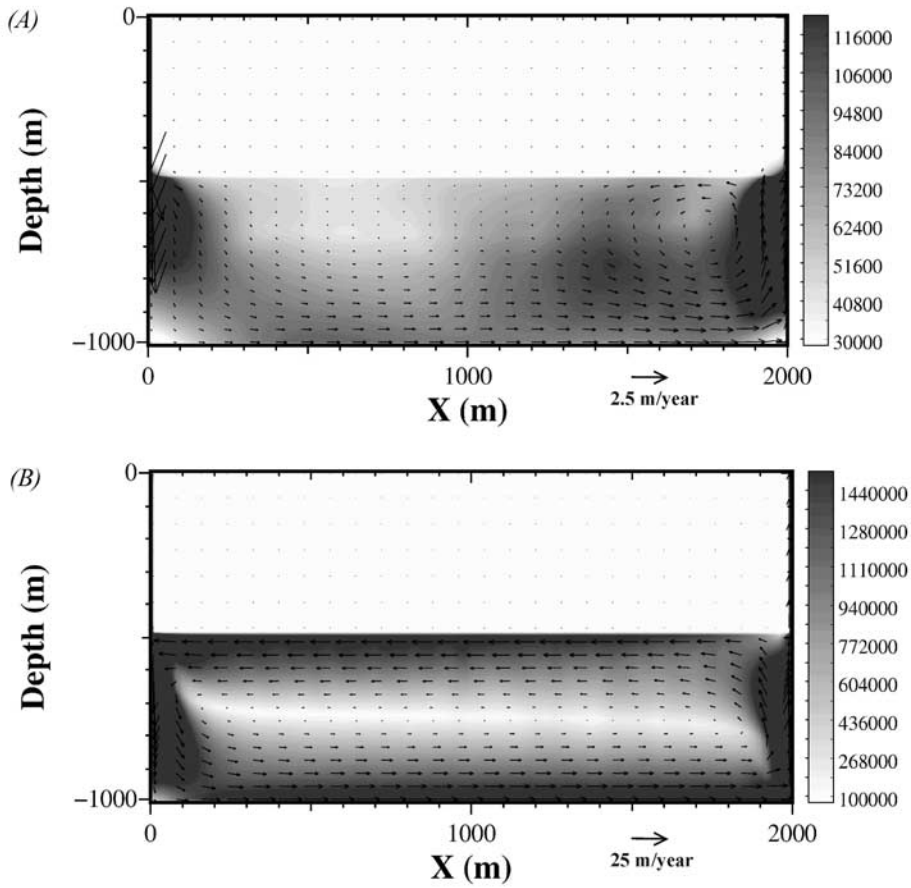

Figure 9. Water/rock ratios (fluid mass (kg)/volume of rock (m^3)) and flow fields at 20,000 years—basement permeability (a) 1×10^{-15} m^2 and (b) 1×10^{-13} m^2.

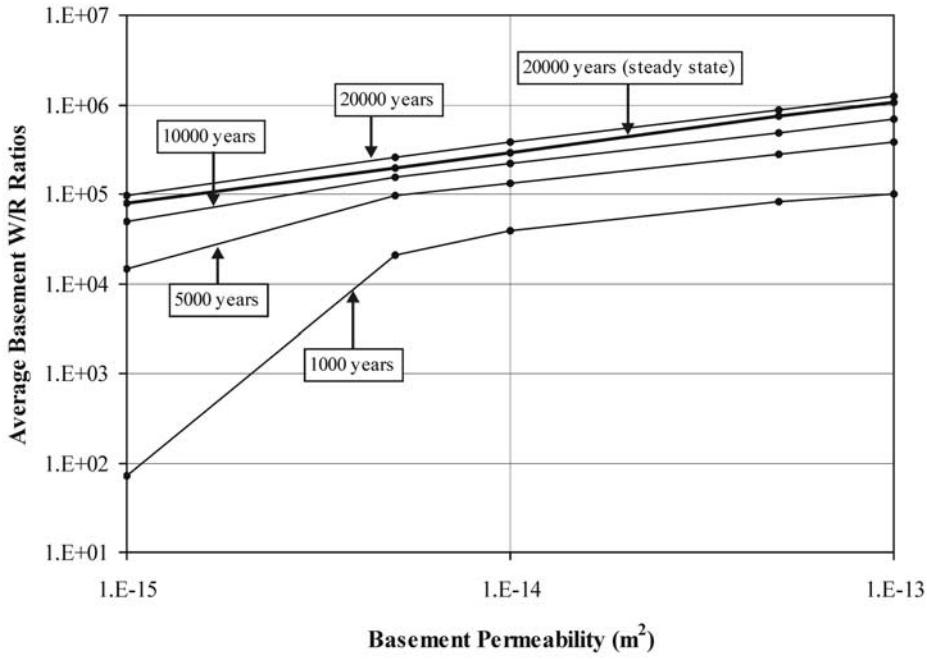

Figure 10. Average basement water/rock ratios (kg/m^3) versus permeability at various times for full transient and steady-state flow simulation (20,000 years).

transient simulation at four different times (1000, 5000, 10,000, and "near" steady state at 20,000 years) and one for 20,000 years of steady-state flow. The steady-state-only result plots as a straight line. The curves showing snapshots of average w/r ratios during the transient state indicate that as time progresses the curves become increasingly log-log linear, approaching the slope of the steady-state curve. The initial slope reflects the slow onset of fluid motion at low permeabilities. At 20,000 years the slopes of the transient and the steady-state simulation are quite similar. The transient curve, however, is offset toward higher w/r ratio values, which is a consequence of the initial higher flow rates. The difference between average water/rock ratios for 20,000 years of transient flow and for the same period of time of steady-state flow increases with basement permeability. Taking into account the shorter transient state at higher permeabilities, the fluid volumes passing through the system in stage 1 are indeed significant.

[39] The log-log linear correlation between average w/r ratios and the basement permeability at steady state is a consequence of the linear correlation between the fluid velocity and the permeability of the medium on the one hand, and the linear increase of w/r ratios with time on the other. If the fluid velocity was proportional to the permeability, the slope of the curve would be equal to one. The slope of about 0.4 indicates that for a given increment in the basement permeability, the average velocity, and thus the average w/r ratios, increases at a slower rate. The exact nature of this correlation remains to be investigated. Nevertheless, average w/r ratios may be a useful way of constraining estimates of bulk permeability. The main limitation to exploiting this type of information will be the derivation of constraints on the elapsed time of convective circulation.

8. Conclusions

[40] For an open, sedimented-ridge setting we have investigated by means of transient numerical simulations the hydrologic factors that can influence chemical signatures of mineral alteration, and how these features are related to permeability. The transient state we consider can be divided into three stages: (1) flow is initiated from a static condition and conductive thermal field, and small, unstable convection cells of low aspect ratio develop; (2) the flow field evolves into a single large convection cell as ingressing seawater migrates across the basement to the discharge site; and (3) a stable convection pattern forms as the effects of the initial thermal condition dissipates and the system attains the steady-state condition. All three stages are shorter and the vigor of convection is higher for higher basement permeability. Despite vigorous fluid flow at high basement permeabilities, thermal homogenization leads to low temperature changes of the fluid along its flow path and thus a greater likelihood that the fluid composition is buffered uniformly by the rock composition. Thus, the time-integrated effects of stages 1 and 2 on the overall intensity of alteration may not be correlative with the vigor of flow.

[41] The unstable flow geometry during stages 1 and 2 is reflected in fluctuations of recharge and discharge rates into and out of the basement, and periodic variations in temperature of the discharging fluids. With the beginning of stage 3, an overall decline of both recharge and discharge rates and discharge temperature begins. The fluid discharge at steady state is approximately one half of that occurring during stage 1. The temperature of vent fluids does not appear to be primarily dependent on the magnitude of the basement permeability or the overall vigor of convection in the basement.

[42] In stage 3, the convective system is similar to a single pass loop, in which fluids that recharge the basement exit after a single pass. At higher permeability, a relatively small region of the basement is affected by interaction between seawater and the rock. In addition, fluid fluxes through the sediment cover are small and would be unlikely to impart a significant chemical signature to the vent fluids. Most of the basement, as well as the deeper sediments surrounding the discharge zone, is part of a hydrologically isolated system. This region is also largely isolated in a chemical sense. The extent of the region influenced by seawater recharge is larger at lower basement permeability. Lateral flow of hydrothermal fluids into the sediments along the discharge conduit is likely to result in distinct alteration reactions. However, as the fluxes into the sediments are relatively low, the intensity of alteration is probably weak for long periods of time. The direction and extent of lateral flow at the recharge zone is dependent on basement permeability.

[43] The changing flow patterns during the transient evolution of the hydrothermal system leads to a strongly heterogeneous evolution of water/rock ratios within the basement layer. The early w/r ratios are overprinted as the circulation pattern changes; however at lower permeability the w/r ratio may be in significant disequilibrium with the current flow field. Chemical signatures of the early state of fluid flow may still be preserved in the rock in the form of mineral alteration products. At steady state, the average w/r ratio has a log-log linear relationship with basement permeability. The relationship for the early transient system is offset toward higher average w/r ratios relative to the steady-state curve as a result of the initial vigorous state. The significance of the transient state in terms of total flow rates increases with basement permeability despite the shorter duration of this state at higher permeability.

Appendix A

[44] Specific discharge is given by

$$q = \frac{-k}{\mu_w}(\nabla P - \rho_w g \nabla Z), \tag{A1}$$

where q is specific discharge, k is the permeability of the rock matrix, P is pressure, g is the gravitational acceleration, and Z is the elevation relative to datum. The variables ρ_w and γ_w are the dynamic fluid viscosity and fluid density, respectively, both are temperature-dependent and to a lesser degree pressure-dependent. For the case where the fluid is compressible and the rock mass is incompressible, and thermal equilibrium exists between the fluid and solid matrix, the equation for the conservation of fluid mass can be written as follows:

$$-\nabla\left\{\rho_w \frac{k}{\mu_w}(\nabla P + \rho_w g \nabla Z)\right\} = \phi\rho_w\left(\beta_w \frac{\partial P}{\partial t} + \gamma_w \frac{\partial T}{\partial t}\right), \tag{A2}$$

where T is temperature, ρ is porosity, and β_w and γ_w are the isothermal compressibility and isobaric thermal expansivity of the fluid, respectively.

[45] The equation of heat transport is:

$$\nabla \cdot \left(\lambda_{ij} \nabla T\right) - \nabla \cdot \{\rho_w h_w q\} = \frac{\partial}{\partial t}[\phi \rho_w h_w + (1-\phi)\rho_m h_m], \quad \text{(A3)}$$

where h_w is the enthalpy of the fluid, ρ_m and h_m are the density and enthalpy of the rock, respectively, and λ_{ij} is the effective thermal conductivity of the rock-fluid mixture. The enthalpy of the rock matrix (h_m) is assumed to change linearly with temperature according the relation

$$h_m = c_m * (T - T_0), \quad \text{(A4)}$$

where c_m is the specific heat of the rock matrix and T_0 is standard temperature (273.14K). The effective thermal conductivity λ_{ij} of the rock-fluid mixture is represented as:

$$\lambda_{ij} = \frac{(\alpha_l - \alpha_t) q_i q_j}{|q|} + \alpha_t |q| \delta_{ij} + \phi \lambda_w \delta_{ij} + (1-\phi)\lambda_m \delta_{ij}, \quad \text{(A5)}$$

where α_l and α_t are the longitudinal and transverse dispersivities, respectively, δij is the Kronecker delta, and and are the thermal conductivity of fluid and rock, respectively.

[46] The coupled flow and heat transport code used in this study was developed by M. Ibaraki. Equations (A2) and (A3) are discretized using a finite-volume approach [*Patankar*, 1980]. There are three variables in these equations, fluid pressure (P), enthalpy of the fluid (h_w) and temperature (T). Pressure and either enthalpy or temperature are used as primary variables. If the temperature of a node is specified explicitly, temperature is a primary variable, otherwise it is the fluid enthalpy. The two governing equations for the two unknowns, that is pressure and either temperature or enthalpy, are solved simultaneously at each grid node at each time step using the Newton-Raphson method. The scheme fully accounts for density changes of the fluid, making the Boussinesq approximation unnecessary. Details on the numerical solution, presented in the context of a solute transport equation rather than a heat transport equation, are available in *Ibaraki* [1998].

[47] **Acknowledgments.** This study was supported by a grant from the Natural Sciences and Engineering Research Council of Canada. Thanks are extended to M. Ibaraki for advice during the implementation of the computer code.

References

Alt-Epping, P., Insights into the evolution of an oceanic hydrothermal system and a method for constraining estimates of the vigor of hydrothermal convection, Ph.D. thesis, The Univ. of B. C., Vancouver, Canada, B. C., 321 pp., 2000.

Alt-Epping, P., and L. Smith, Computing geochemical mass transfer and water/rock ratios in submarine hydrothermal systems: Implications for estimating the vigor of convection, *Geofluids*, *1*, 163–181, 2001.

Becker, K., et al., Deep drilling into young oceanic crust, Hole 504B, Costa Rica Rift, *Rev. Geophys.*, *27*, 79–102, 1989.

Becker, K., R. H. Morin, and E. E. Davis, Permeabilities in the Middle Valley hydrothermal system measured with packer and flowmeter experiments, in *Proceedings of the Ocean Drilling Program, Scientific Results*, vol. 139, pp. 613–627, College Station, Tex., 1994.

Bessler, J. U., L. Smith, and E. E. Davis, Hydrologic and thermal conditions at a sediment/basalt interface: Implications for interpretation of field measurements at Middle Valley, in *Proceedings of the Ocean Drilling Program, Scientific Results*, vol. 139, pp. 667–679, College Station, Tex, 1994.

Bodvarrson, G., and R. P. Lowell, Ocean-floor heat flow and the circulation of interstitial waters, *J. Geophys. Res.*, *77*, 4472–4475, 1972.

Cann, J. R., and M. R. Strens, Modeling periodic megaplume emissions by black smoker systems, *J. Geophys. Res.*, *94*, 12,227–12,237, 1989.

Cathles, L., A capless 350°C flow zone model to explain megaplumes, salinity variations, and high temperature veins in ridge axis hydrothermal systems, *Econ. Geol.*, *88*, 1977–1988, 1993.

Christensen, N. I., and R. Ramananantoandro, Permeability of the oceanic crust based on experimental studies of basalt permeability at elevated pressures, *Tectonophysics*, *149*, 181–186, 1988.

Davis, E. E., and H. Villinger, Tectonic and thermal structure of the Middle Valley sedimented rift, northern Juan de Fuca Ridge in *Proceedings of the Ocean Drilling Program, Initial Results.*, vol. 139, pp. 9–41, College Station, Tex., 1992.

Davis, E. E., J. Mottl, and A. T. Fisher (Eds.), *Proceedings of the Ocean Drilling Program, Initial Results*, vol. 139, College Station, Tex., 1992.

Davis, E. E., J. Mottl, and A. T. Fisher (Eds.), *Proceedings of the Ocean Drilling Program, Scientific Results*, vol. 139, College Station, Tex., 1994.

Davis, E. E., D. S. Chapman, and C. B. Forster, Observations concerning the vigor of hydrothermal circulation in young volcanic crust, *J. Geophys. Res.*, *101*, 2927–2942, 1996.

Davis, E. E., K. Wang, J. He, D. S. Chapman, H. Villinger, and A. Rosenberger, An equivocal case for high Nusselt-number hydrothermal convection in sediment-buried igneous oceanic crust, *Earth Planet. Sci. Lett.*, *146*, 137–150, 1997.

Davis, E. E., D. S. Chapman, K. Wang, H. Villinger, A. T. Fisher, S. W. Robinson, J. Grigel, D. Pribnow, J. Stein, and K. Becker, Regional heat-flow variations across the sedimented Juan de Fuca Ridge eastern flank: Constraints on lithospheric cooling and lateral hydrothermal heat transport, *J. Geophys. Res.*, *104*(B8), 17,675–17,688, 1999.

Ferry, J., Fluid interaction between granite and sediment during metamorphism, south-central Maine, *Am. J. Sci.*, *278*, 1025–1056, 1978.

Fisher, A. T., Permeability within the basaltic oceanic crust, *Rev. Geophys.*, *36*(2), 143–182, 1998.

Fisher, A. T., and K. Becker, The correlation between heat flow and basement relief: Observations and numerical examples and implications for upper crustal permeability, *J. Geophys. Res.*, *100*, 12,641–12,657, 1995.

Fisher, A. T., K. Fischer, D. Lavoie, M. Langseth, and J. Xu, Geotechnical and hydrogeological properties of sediments from Middle Valley, northern Juan de Fuca Ridge in *Proceedings of the Ocean Drilling Program, Scientific Results*, vol. 139, College Station, Tex., 1994.

Fouquet, Y., R. A. Zierenberg, and D. J. Miller (Eds.) *Proc. Ocean Drilling Program, Initial Results*, vol. 169, College Station, Tex., 1998.

Gillis, K. M., and P. T. Robinson, Patterns and processes of alteration in lavas and dykes of the Troodos Ophiolite, Cyprus, *J. Geophys. Res.*, *95*, 21,523–21,548, 1990.

Hamano, Y., Physical properties from basalts from Hole 417D and 418A, *Initial Rep. Deep Sea Drilling Proj.*, *51–53*, 1457–1466, 1980.

Ibaraki, M., A robust and efficient numerical model for analyses of dependent flow in porous media, *J. Contam. Hydrol.*, *34*, 235–246, 1998.

Ibaraki, M., and L. Smith, Numerical modeling of hydrothermal convection in a ridge-axis setting, *Geol. Soc. Am. Annu. Meet., Abstr.*, 1997.

Karato, S., Physical properties of basalts from the Galapagos, Leg 70, *Initial Rep. Deep Sea Drilling Proj.*, *69*, 687–695, 1983.

Larson, R. L., A. T. Fisher, and R. Jarrard, Highly layered and permeable Jurassic oceanic crust in the western Pacific, *Earth Planet. Sci. Lett.*, *119*, 71–83, 1993.

Leybourne, M. I., and W. D. Goodfellow, Mineralogy and mineral chemistry of hydrothermally altered sediment, Middle Valley, Juan de Fuca Ridge in *Proceedings of the Ocean Drilling Program, Scientific Results*, vol. 139, pp. 155–207, College Station, Tex., 1994.

Lister, C. R. B., An explanation for the multivalent heat transport found experimentally for convection in a porous medium, *J. Fluid Mech.*, *214*, 187–320, 1990.

Lowell, R. P., and L. N. Germanovich, Dike injection and the formation of megaplumes at ocean ridges, *Science*, *267*, 1804–1807, 1995.

Lowell, R. P., and P. A. Rona, Hydrothermal models for the generation of massive sulfide deposits, *J. Geophys. Res.*, *90*, 8769–8783, 1985.

Meyer, C. A., R. B. McClintock, G. J. Silverstri, and J. R. C. Spencer, *ASME Steam Tables: Thermodynamic and Transport Properties of Steam*, 6th ed., Am. Soc. Mech. Eng., New York, N. Y., 1983.

Norton, D., Sourcelines, sourceregions, and pathlines for fluids in hydrothermal systems related to cooling plutons, *Econ. Geol.*, *73*, 21–28, 1978.

Patankar, S. V., *Numerical Heat Transfer and Fluid Flow*, p. 197, Taylor and Francis, New York, 1980.

Rabinowicz, M., J. Boulegue, and P. Genthon, Two- and three-dimensional modeling of hydrothermal convection in the sedimented Middle Valley segment, Juan de Fuca Ridge, *J. Geophys. Res.*, *103*, 24,045–24,065, 1998.

Ribando, R., K. Torrence, and D. Turcotte, Numerical models for hydrothermal circulation in the oceanic crust, *J. Geophys. Res.*, *81*, 3007–3012, 1976.

Rigsby, C. A., R. A. Zierenberg, and P. A. Baker, Sedimentary and diagenetic structures and textures in turbiditic and hemiturbiditic strata as revealed by whole-core X-radiography, Middle Valley, northern Juan de Fuca Ridge in *Proceedings of the Ocean Drilling Program, Scientific Results*, vol. 139, pp. 105–113, College Station, Tex., 1994.

Rosenberg, N. D., F. J. Spera, and R. M. Haymon, The relationship between flow and permeability field in seafloor hydrothermal systems, *Earth Planet. Sci. Lett.*, *116*, 135–153, 1993.

Stein, J. S., and A. T. Fisher, Multiple scales of hydrothermal circulation in Middle Valley, northern Juan de Fuca Ridge: Physical constraints and geologic models, *J. Geophys. Res.*, *106*, 8563–8580, 2001.

Taylor, H. P., Jr., Water/rock interactions and the origin of H_2O in granitic batholiths, *J. Geol. Soc. London*, *133*, 509–558, 1977.

Valley, J., Stable isotope geochemistry of metamorphic rocks, in *Stable Isotopes, Reviews in Mineralogy*, vol. 16, edited by Valley et al., Mineralogical Society of America, Washington, D. C., 1986.

Von Damm, K. L., Controls on the chemistry and temporal variability of seafloor hydrothermal fluids, in *Seafloor Hydrothermal Systems: Physical, Chemical, Biological, and Geological Interactions*, *Geophys. Monogr. Ser.*, 91, edited by Humphris et al., pp. 222–247, AGU, Washington, D. C., 1995.

P. Alt-Epping, CSIRO—Exploration and Mining, ARRC, P.O. Box 1130, Bentley, Western Australia 6102, Australia. (Peter.Alt-Epping@csiro.au)

L. Smith, Department of Earth and Ocean Sciences, University of British Columbia, 6339 Stores Road, Vancouver, British Columbia, Canada V6T 1Z4. (lsmith@eos.ubc.ca)